Fusion cross sections for four heavy-ion entrance channels leading to the ^{23}Na compound nucleus

J. F. Mateja, J. Garman,* D. E. Fields, and R. L. Kozub
Department of Physics, Tennessee Technological University, Cookeville, Tennessee 38505

A. D. Frawley and L. C. Dennis
Department of Physics, Florida State University, Tallahassee, Florida 32306
(Received 19 December 1983)

Excitation functions for the yields of residual nuclei from the ^{7}Li + ^{16}O and ^{9}Be + ^{14}N reactions have been measured for ^{7}Li and ^{14}N laboratory bombarding energies of 12 to 34 MeV and 15 to 63 MeV, respectively. Beginning at Coulomb barrier energies, we find that the total fusion cross section diverges from the total reaction cross section obtained from optical model fits to elastic scattering data. This indicates that the process responsible for fusion cross section limitations in this mass region begins near the Coulomb barrier and becomes progressively more important as the bombarding energy is increased. Comparison of the critical angular momenta deduced from the total fusion cross sections for these and two previously investigated entrance channels which form the ^{23}Na compound nucleus, ^{11}B + ^{12}C and ^{10}B + ^{13}C, rules out a compound nucleus limitation at these energies. A systematic study of fusion cross sections in this mass and energy region, together with the results of a previous study of the light particles produced in the ^{11}B + ^{12}C and ^{10}B + ^{13}C reactions, suggests that competition for entrance channel flux by reactions producing light particles with projectilelike velocities is primarily responsible for the fusion cross section limitations.

I. INTRODUCTION

Understanding the mechanism responsible for producing fusion cross section limitations for nuclei in the $1p$ and $2s$-$1d$ shells has been the aim of a number of experimental and theoretical studies over the past decade.[1-9] Despite the attention given to this problem, the question of whether the fusion cross section limitation arises because of a feature of the entrance channel nuclei, or because of some property of the compound nucleus, remains unresolved. In an attempt to determine the mechanism responsible for these low-energy fusion cross section limitations, we have undertaken a study of four entrance channels which lead to the same compound nucleus, ^{23}Na. The results from our study of two of these entrance channels, ^{11}B+^{12}C and ^{10}B+^{13}C, have been presented in earlier publications.[10,11] The results from the remaining two entrance channels, ^{7}Li+^{16}O and ^{9}Be+^{14}N, are presented here along with a comparison of all four systems. The behavior of the critical angular momenta for fusion of these four systems appears to rule out a compound nucleus limitation, such as the yrast or "statistical" yrast line,[4] at these energies. An earlier investigation of the fast light particles produced in the ^{11}B+^{12}C and ^{10}B+^{13}C reactions[12] and a systematic study of fusion cross sections in this mass and energy region suggest, on the other hand, that projectile fragmentation competes strongly for entrance channel flux, thereby limiting the fusion cross section.

II. EXPERIMENTAL PROCEDURES

Beams of ^{7}Li and ^{14}N were provided by the Florida State University super-FN tandem Van de Graaff accelerator. The ^{7}Li beam was accelerated over a laboratory energy range from 12 to 34 MeV, while the ^{14}N beam spanned an energy range from 15 to 63 MeV. The heavy evaporation residues emitted from the ^{7}Li+^{16}O and ^{9}Be+^{14}N reactions were mass identified by measuring flight times along a 2.7 m flight path. A microchannel plate detector marked the initial passage of the heavy residues. A 450 mm silicon surface barrier detector was used to obtain the stop and full energy signal for each residue. The time resolution obtained with this system, 450 psec, was sufficient to produce unit mass resolution over our entire energy range. The efficiency of the time-of-flight system can vary, due to the changing number of electrons produced in the start detector by different mass and energy residues. This efficiency was checked experimentally by comparing elastic scattering peaks in the single's surface barrier detector energy spectra to the corresponding peaks in the time-of-flight versus energy coincidence spectra. Over the energy range of interest, the start detector was found to be at least 98% efficient for residue masses ≥ 10, the residue masses for which fusion events were observed.

For the ^{7}Li + ^{16}O experiment, self-supporting targets of SiO_2 were used. A typical two-dimensional mass versus energy spectrum from this study is shown in Fig. 1. As can be seen in Fig. 1, the silicon in the target presented no identification problems as the heavy residues arising from the decay of the ^{7}Li+^{28}Si compound system were well separated from the residues resulting from the decay of the ^{7}Li+^{16}O compound system. For the ^{14}N+^{9}Be study, aluminum-backed ^{9}Be targets were used. Events arising from the ^{14}N+^{27}Al reaction were, as in the previous case, well separated from the events of interest. A contaminant on this target whose residues could not be

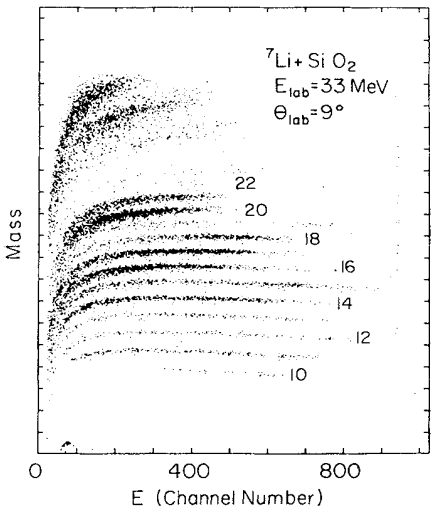

FIG. 1. A representative mass versus energy contour map for the ^{7}Li+^{16}O system.

separated from the residues of interest was ^{16}O. To allow a proper contaminant subtraction, the ^{14}N+^{16}O fusion cross section was measured at all of the energies and angles which were measured in the ^{9}Be+^{14}N experiment.

The total cross sections for residues with $A > 10$ were obtained by integrating the angular distributions for each mass group over the energies and angles shown in Table I. While complete angular distributions were measured at several energies, excitation functions were measured in finer energy steps (1.0 and 1.5 MeV energy intervals for the ^{7}Li+^{16}O and ^{9}Be+^{14}N studies, respectively) at a fixed angle near the maximum value of $(d\sigma/d\Omega)\sin\theta$. Since the shapes of the fusion angular distributions change slowly as a function of bombarding energy,[5,11,13] the measured angular distributions were interpolated and used to derive the total fusion cross sections σ_{fus} from the single angle yields.

The absolute cross section for the ^{9}Be+^{14}N experiment was obtained by measuring the product of target thickness and solid angle $N_T\Omega$ by elastically scattering ^{16}O from the ^{9}Be target. At an ^{16}O bombarding energy of 13 MeV and at angles of 20° and less, the ratio of the scattered cross section to Rutherford was found to be constant as a function of angle, indicating the scattering was Rutherford. For the ^{16}O target used in the ^{7}Li+^{16}O experiment, a 15 MeV ^{12}C beam, scattered at angles of 18° and 20°, was used for the target thickness determination. At this bombarding energy and at these angles, we have found that the scattering of ^{12}C from ^{16}O is Rutherford.

Using the criteria outlined in our ^{11}B+^{12}C and ^{10}B+^{13}C study,[11] the energy spectra of all mass groups were inspected for evidence of nonfusion events before a fusion cross section was calculated for any residue mass. In general, channels which contain both fusion and nonfusion events display a low-energy group characteristic of evaporation residues and a component at higher energy whose velocity is near that of the projectile. The higher energy component can arise from a variety of reaction mechanisms, among which are direct reactions involving nuclear transfer between the target and projectile, particle emission from a projectile which has been excited in a peripheral collision, or inelastic scattering. To assist in the discrimination between fusion and nonfusion events, each exit channel energy spectrum was compared among the four entrance channels. When this comparison is made at the same compound nucleus excitation energy, the shapes of the fusion evaporation residue energy distributions should be similar. The presence of a nonfusion component in any one system should cause a readily apparent difference in the energy spectrum for that system.

Using these criteria, there was no evidence for any nonfusion strength in the ^{7}Li+^{16}O experiment. There was, however, evidence for some direct transfer strength in the mass 15 residues from the ^{9}Be+^{14}N reaction (see Fig. 2). This is due to a single particle pickup by the ^{14}N projectile. These events were readily identifiable as nonfusion because of their projectilelike velocities and because such events do not occur in the mass 15 energy spectra for any other entrance channel. They have been excluded in our evaluation of the fusion cross section for the mass 15 exit channel and for the total fusion cross section.

The mass 14 exit channel in the ^{9}Be+^{14}N experiment also required special attention. The extraction of the fusion cross section for this mass group was complicated by the presence of a strong elastic and inelastic scattering component. It is difficult, if not impossible, to extract a reliable fusion yield from the energy spectrum under these conditions. The approach we have taken here is based upon the observation that the mass 14 cross section, when plotted as a function of ^{23}Na excitation energy for the three entrance channels where there is no interference

TABLE I. Energies and angles measured for the present study.

Reaction	Laboratory bombarding[a] energies (MeV)	Laboratory angles (deg)
^{9}Be+^{14}N	15, 24, 33, 42, 51, 57	4.5, 6.5, 8.5,[b] 11.5, 14.5, 17.5, 20.5, 24.5, 29.5, 34.5, 39.5, 44.5
^{7}Li+^{16}O	12, 18, 24, 30, 34	5, 7, 9,[b] 12, 15, 18, 21, 25, 30, 35, 40

[a]Energies at which complete angular distributions were measured.
[b]Angle at which the excitation function for each system was measured.

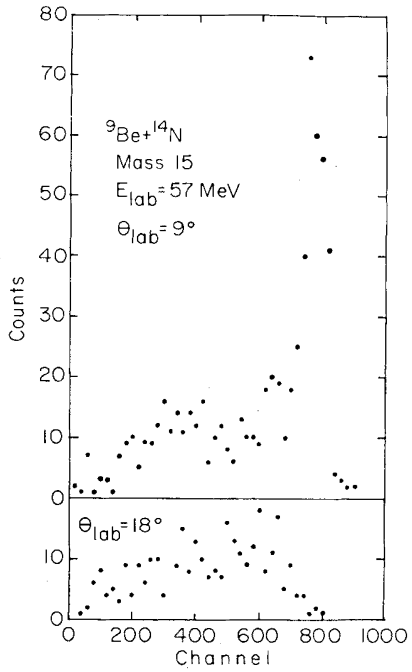

FIG. 2. Energy spectrum of the mass 15 residue in the ^{9}Be+^{14}N reaction. The transfer component apparent at 9° is essentially gone by 18°.

from inelastic scattering, has only a weak dependence on entrance channel. This can be seen in Fig. 3 where the energy dependence of the mass 14 group is plotted for the ^{11}B+^{12}C, ^{10}B+^{13}C, and ^{7}Li+^{16}O entrance channels. The weak dependence on entrance channel of the mass 14 group and several of the other exit channels will be discussed in greater detail later in this paper. In computing the ^{9}Be+^{14}N total fusion cross section, we have used the average mass 14 cross section at each energy obtained from the data in Fig. 3.

As mentioned previously, an ^{16}O contaminant was present on the ^{9}Be target in the ^{14}N+^{9}Be experiment. To allow a proper contaminant subtraction, the ^{14}N+^{16}O fusion cross section was measured at all energies and angles measured in the ^{14}N+^{9}Be experiment. For the ^{14}N+^{16}O study, a self-supporting SiO_2 target was used. Mass groups which were common to both the ^{14}N+^{16}O and ^{14}N+^{9}Be experiments and which contained yield

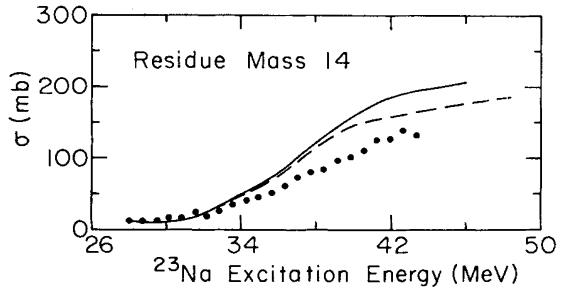

FIG. 3. Energy dependence of the mass 14 residue. The energy dependence of the mass 14 residue for the ^{11}B+^{12}C, ^{10}B+^{13}C, and ^{7}Li+^{16}O entrance channels are shown as solid, dashed, and dotted lines, respectively.

were $A=16$ (primarily due to the recoiling target nucleus), 18, 20, 21, and 22. In addition, in the ^{14}N+^{16}O study, yield was observed for masses 23—29. Yields from these mass groups (23—29) were use to normalize the two experiments. While essentially no contribution to the experimentally measured yield could be attributed to the ^{14}N+^{16}O reaction at our lowest bombarding energies, approximately 10% of the total yield at our highest bombarding energies arose from the ^{16}O contaminant. The ^{9}Be+^{14}N cross sections reported in this work have had the contaminant yields removed on a mass by mass basis.

Finally, the uncertainties in the total fusion cross sections for both experiments are attributable to counting statistics (3%), angle setting uncertainties (4%), identification of fusion products (3%), extrapolation of the data to zero degrees and beyond 40° (4%), normalization of the single-angle excitation functions to the angular distributions (3%), and errors in measuring the absolute target thickness (8%). The total uncertainty in the absolute cross sections is therefore approximately 11%.

III. EXPERIMENTAL RESULTS AND DISCUSSION

Excitation functions for the evaporation residues produced by the ^{7}Li+^{16}O and ^{9}Be+^{14}N entrance channels are presented in Figs. 4 and 5. The behavior of these excitation functions appears to be in qualitative agreement with a fusion-evaporation process. If we assume that the evaporation of protons, neutrons, and alpha particles dominates the compound nucleus decay process, the energy dependence of the cross sections for the various mass groups presented in Figs. 4 and 5 can be understood in terms of the competition between the energetically allowed exit channels. The assumption that d, t, and ^{3}He emission from the compound nucleus is small is supported by two recent experimental studies in this mass and energy region.[13,14] The available decay channels and the energy at which each entrance channel forms the compound nucleus are presented in Fig. 6. As can be seen in this figure, there are different energy thresholds below which a particular number of light particles cannot be emitted (these thresholds correspond to the energies required to form the ground states of the relevant heavy residues). Once the energy threshold for the emission of a particular number of light particles has been exceeded, the cross section to the residues in that group would be expected to increase rapidly as the level density in each residue begins to increase. Furthermore, the mass groups corresponding to one, two, three, four, and five particle emission will peak at successively higher energies, each group reaching a maximum near the energy at which the next group begins to show a significant yield. It is clear in Figs. 4 and 5 that the experimental excitation functions exhibit the expected characteristics at the appropriate energies.

The decay cross sections for the ^{7}Li+^{16}O and the ^{9}Be+^{14}N entrance channels are compared with each other in Fig. 7. Also included in this figure are the cross sections for the ^{11}B+^{12}C (solid curve) and the ^{10}B+^{13}C (dashed curve) entrance channels which were taken from Ref. 11. An interesting feature of the data is that while

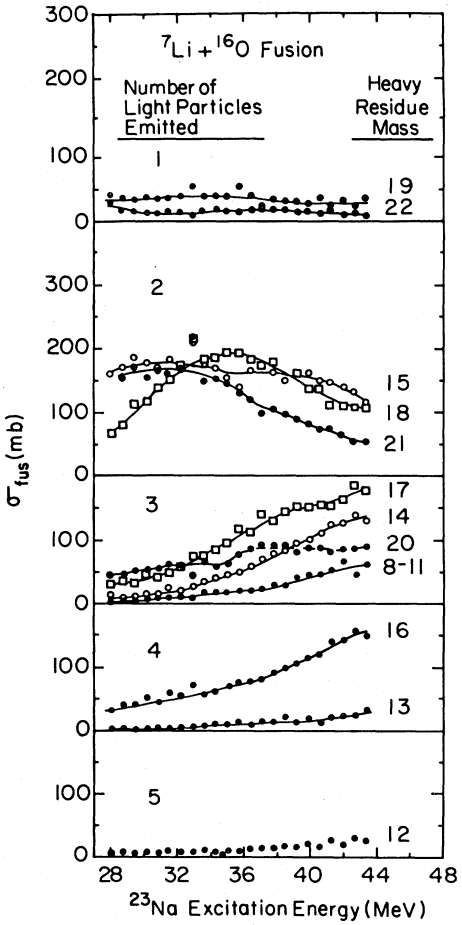

FIG. 4. Excitation functions of the heavy residues produced in the ^{7}Li+^{16}O reaction. The lines are drawn only to help guide the eye. The relative uncertainties due to counting statistics are approximately twice the size of each data point.

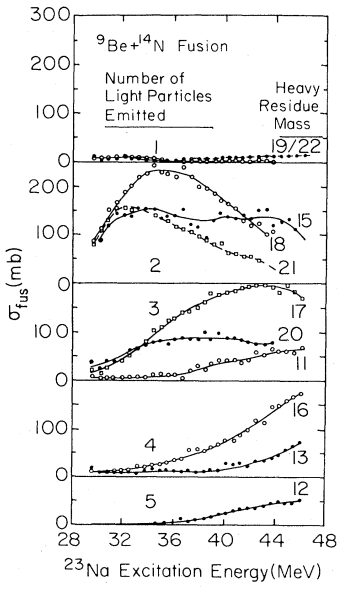

FIG. 5. Excitation functions of the heavy residues produced in the ^{9}Be+^{14}N reaction. The lines are drawn only to help guide the eye. The relative uncertainties due to counting statistics are approximately twice the size of each data point.

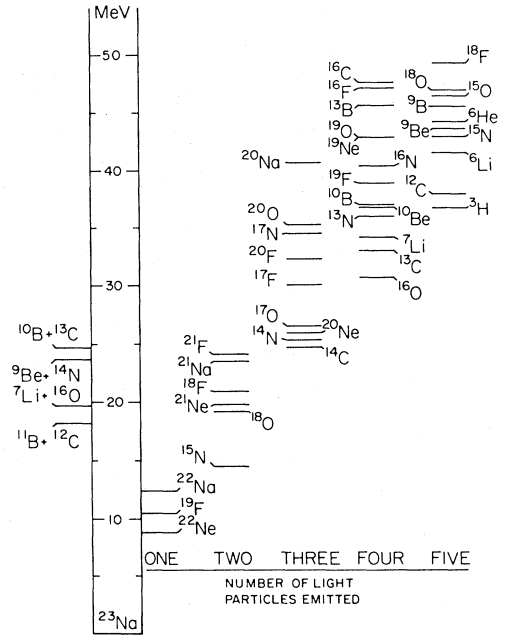

FIG. 6. Ground states of the residual nuclei available for the decay of the ^{23}Na compound nucleus. The residual nuclei have been grouped according to the number of light particles which must be emitted to reach a particular decay channel (assuming neutron, proton, and alpha particle emission only).

there is a marked difference in the decay cross sections to masses 15, 18, and 21 among the various entrance channels, the cross sections for the remaining exit channels are less dependent on entrance channel. These features of the data can be understood in terms of the angular momentum brought into the compound nucleus by each entrance channel, and in terms of the decay channels available to

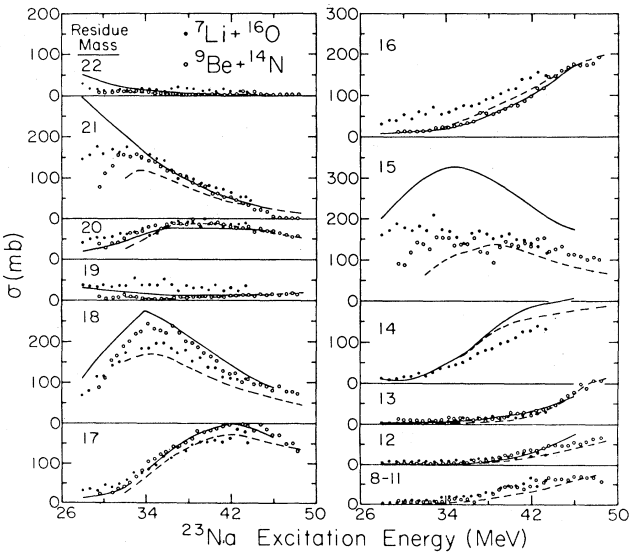

FIG. 7. Angle-integrated cross sections for the evaporation residues produced in the ^{7}Li+^{16}O and ^{9}Be+^{14}N reactions. Also displayed in this figure are the angle integrated cross sections for the residues arising from the ^{11}B+^{12}C entrance channel (solid lines) and the ^{10}B+^{13}C entrance channel (dashed lines).

the compound nucleus at a particular compound nucleus excitation energy.

The center-of-mass energy of an entrance channel at a particular compound nucleus excitation energy determines the range of angular momentum values available to the compound nucleus. To reach a ^{23}Na excitation energy of 32 MeV, for example, it is clear from Fig. 6 that the ^{11}B+^{12}C entrance channel requires the greatest center-of-mass energy since this entrance channel has the lowest capture Q value. Of the four entrance channels, the ^{10}B+^{13}C would require the smallest center-of-mass energy. As a consequence, the ^{11}B+^{12}C entrance channel brings the largest range of angular momenta into the compound nucleus at this excitation energy (from $0\hbar$ up to some maximum value), while ^{10}B+^{13}C brings in the smallest. This observation is consistent with the results one obtains if the critical angular momenta are extracted from the total fusion cross sections for the various entrance channels according to the sharp-cutoff approximation

$$\sigma_{\rm fus}=\pi\lambda^2\sum_{l=0}^{l_{\rm cr}}(2l+1)\ . \tag{1}$$

At a ^{23}Na excitation energy of 32 MeV, the critical angular momenta for the ^{11}B+^{12}C, ^{7}Li+^{16}O, ^{9}Be+^{14}N, and ^{10}B+^{13}C systems are $9.8\hbar$, $7.6\hbar$, $5.9\hbar$, and $4.0\hbar$, respectively. The difference in the mass 15, 18, and 21 decay cross sections for the four entrance channels at this ^{23}Na excitation energy (see Fig. 7) appears to be due to these angular momenta differences and the available decay channels. While the high angular momenta brought into the compound nucleus by the ^{11}B+^{12}C entrance channel (and not by the ^{10}B+^{13}C, for example) will be shared among all the energetically allowed decay channels, it is clear from Fig. 6 that not all decay channels are available. At 32 MeV, the four- and five-particle decay channels are energetically closed. While some of the three-particle decay channels are open, the energy and, consequently, the angular momentum which can be removed from the compound nucleus through particle decays to these exit channels are small. This requires, then, that the one- and two-particle emission channels remove most of the high spin flux at a ^{23}Na excitation energy of 32 MeV. The decay of a high angular-momentum, compound-nucleus state to a mass 15, 18, or 19 residue is further favored since it involves alpha particle emission. A substantial mass 19 cross section is not expected, however, because at this energy one is well above the 4.7 MeV alpha emission threshold in ^{19}F. The high angular momentum flux must appear, therefore, in residue masses 15, 18, and 21. It is in these mass groups that the ^{11}B+^{12}C entrance channel, the system with the largest angular momentum range at this energy, has a cross section which is substantially larger than the cross sections for the other entrance channels. The system with the smallest angular momentum range, the ^{10}B+^{13}C, has the smallest cross sections for these masses.

The remaining exit channels have cross sections which do not depend on entrance channel. This suggests that decays to these residues arise from compound nucleus states having low angular momenta, angular momenta which would be brought into the compound nucleus by all entrance channels.

Displayed in Figs. 8 and 9 are the total fusion cross sections and the total reaction cross sections for the ^{7}Li+^{16}O and ^{9}Be+^{14}N systems, respectively. The total reaction cross sections were determined from optical model parameters reported for these systems in the literature.[15,16] These optical model parameters, shown in Table II, were obtained by fitting elastic scattering angular distributions or excitation functions which spanned wide energy ranges. It is expected, therefore, that the energy dependence of the total reaction cross sections is accurately predicted.

When Figs. 8 and 9 are compared, it is apparent that the total fusion cross section is significantly smaller than the total reaction cross section for both entrance channels. Similar results were observed in our earlier work on ^{11}B+^{12}C and ^{10}B+^{13}C (Ref. 11) and have also been reported in studies of ^{9}Be+^{28}Si, ^{6}Li+^{12}C, ^{6}Li+^{13}C, ^{7}Li+^{12}C, and ^{7}Li+^{13}C.[13,17] In all cases, the process responsible for the fusion cross section limitation apparently begins at very low energies (energies near the Coulomb barrier) and becomes more important at higher energies, as evidenced by an increase in the separation of the fusion and total reaction strengths.

The total fusion cross section, as discussed earlier, may also be used to estimate the maximum angular momentum associated with the fusion process. This angular momentum, commonly called the critical angular momentum, has been extracted from the fusion data according to Eq. (1). The energy dependence of the critical angular momenta for the ^{7}Li+^{16}O and ^{9}Be+^{14}N entrance channels is presented in Figs. 10 and 11, respectively. The grazing angular momenta for these systems (solid lines), obtained from the optical model parameters listed in Table II, are also shown in these figures as a function of the compound nucleus excitation energy. The critical angular momentum for each system begins to diverge from the grazing angular momentum at our lowest bombarding energy. Again, this is an indication that the process limiting the fusion cross section begins at very low energies and be-

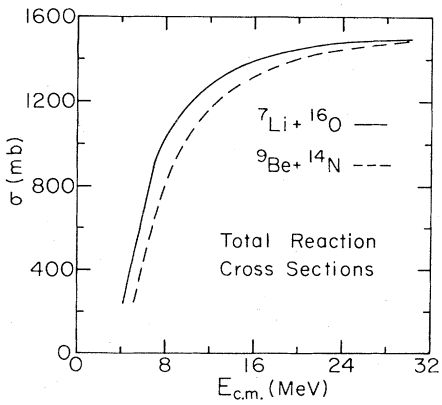

FIG. 8. Total reaction cross section versus center-of-mass energy for the ^{7}Li+^{16}O and ^{9}Be+^{14}N entrance channels. The total reaction cross sections were determined from optical model parameters reported for these systems in Refs. 15 and 16.

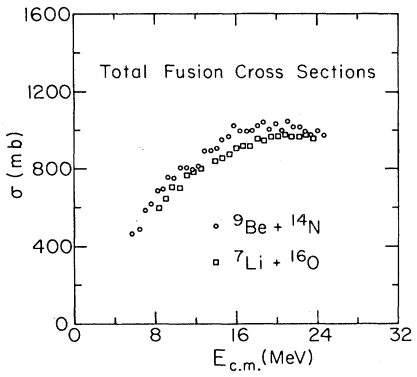

FIG. 9. Total fusion cross sections versus center-of-mass energy for the ^{7}Li+^{16}O and ^{9}Be+^{14}N entrance channels.

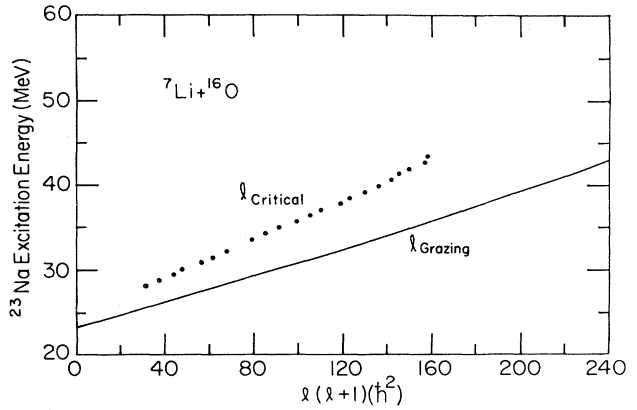

FIG. 10. The critical angular momenta for the ^{7}Li+^{16}O entrance channel versus ^{23}Na excitation energy. The grazing angular momentum line was determined from the optical model parameters reported in Ref. 15.

comes increasingly important at higher energies.

In the energy region studied, the results presented in Figs. 10 and 11 clearly indicate that the ^{7}Li+^{16}O and the ^{9}Be+^{14}N entrance channels are being limited. Similar results have been reported for the ^{11}B+^{12}C and the ^{10}B+^{13}C systems.[10,11] While there are obvious fusion cross section limitations at these energies, a comparison of the critical angular momenta for all four entrance channels shows no evidence of a common limitation in this energy range (see Fig. 12). A common limitation in the critical angular momentum is expected if the limitation in the fusion cross section is due to a compound nucleus property like the compound nucleus yrast or statistical yrast line.[4] While a common limitation may occur at higher energies (there appears to be some evidence for this for three of the systems in Fig. 12), the fact remains that at low energies the systems are being limited and the mechanism responsible does not appear to be related to the yrast or statistical yrast lines. Since this result was first reported for the ^{11}B+^{12}C and ^{10}B+^{13}C entrance channels,[10] similar results have been reported for systems leading to the ^{24}Mg and ^{28}Si compound nuclei.[18,19]

Results obtained from Eq. (1) are often extracted for systems with nonzero channel spin even though it may be more appropriate to include the channel spin in these calculations. The four entrance channels which lead to the ^{23}Na compound nucleus provide a test of the importance of including the entrance channel spin in these calculations because of the diversity of channel spins among the four systems (see Table III). Using the sharp-cutoff model to describe the fusion process, two different values for the critical angular momentum can be extracted from the data depending on whether the cutoff is made on the orbital angular momentum l_{cr}, or on the total angular momentum J_{cr}. The method for extracting l_{cr} has already been discussed [see Eq. (1)] and the results have been presented in Fig. 12. The critical angular momentum J_{cr} may be extracted from the data using the following:

$$\sigma_{fus}(E)=\sum_{J=0}^{J_{cr}}\sigma_J\ , \tag{2}$$

$$\sigma_J=(2J+1)\pi\lambda^2/(2I_1+1)(2I_2+1)\times\sum_{I=|I_1-I_2|}^{I_1+I_2}\ \sum_{l=|J-I|}^{J+I}\theta(l_g-l)\ , \tag{3}$$

where θ is the usual step function, I_1 and I_2 are the target and projectile spins, I is the channel spin, l is the orbital angular momentum, and l_g is the grazing angular momentum. The results from the ^{10}B+^{13}C system, the entrance channel with the largest channel spin and the largest difference in J_{cr} and l_{cr}, are presented in Fig. 13. Even for this entrance channel the difference in J_{cr} and l_{cr} is small. In Fig. 14, the J_{cr} values for the four entrance channels are presented. As can be seen by comparing Figs. 12 and 14, there is little qualitative difference when l_{cr} is compared among the four entrance channels and when J_{cr} is compared.

TABLE II. Optical model parameters used to calculate total reaction cross sections and grazing angular momenta. The radii are parametrized as $R=r(A_p^{1/3}+A_t^{1/3})$.

System	V_0 (MeV)	r_r (fm)	a_r (fm)	W_V (MeV)	W_D (MeV)	r_0 (fm)	a_0 (fm)	r_c (fm)	Laboratory energy range (MeV)	Ref.
^{9}Be+^{14}N	50.	1.310	0.450	10.	0.	1.310	0.450	1.310	7.5—30.7	15
^{7}Li+^{16}O	195.	0.739	0.740	0.	55.	0.739	0.740	1.300	9 —36	16

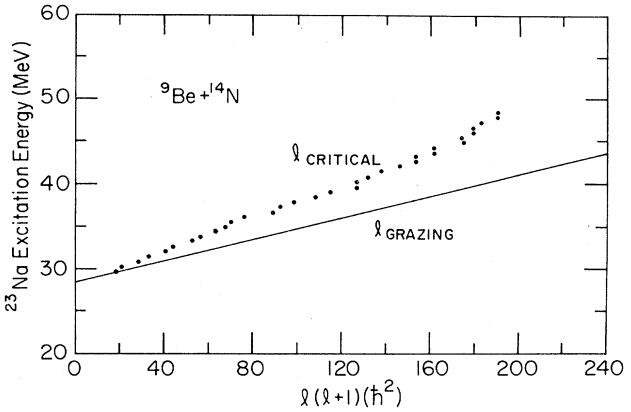

FIG. 11. The critical angular momenta for the ^{9}Be+^{14}N entrance channel versus ^{23}Na excitation energy. The grazing angular momentum line was determined from the optical model parameters reported in Ref. 16.

While the exact nature of the process responsible for the fusion cross section limitations at these energies is still unclear, a recent study[12] of the light particles produced in the ^{11}B+^{12}C and ^{10}B+^{13}C reactions at 54 MeV may provide an important insight into the mechanism primarily responsible for the fusion cross section limitations. The light particles observed in this study had beamlike velocities and were shown to be consistent with projectile breakup. Such a process would certainly reduce or limit the total fusion strength by competing for entrance channel flux. It was demonstrated in this study that the two mechanisms, fusion and projectile breakup, accounted for approximately 85% of the total reaction cross sections for both entrance channels. We expect the remaining strength to reside in the inelastic scattering channel.

It was also found in the ^{11}B+^{12}C and ^{10}B+^{13}C light-particle study that the strongest light-particle exit channels were those involving the weakest projectile two-particle binding energies (see Fig. 12 of Ref. 12). One might, therefore, expect to find reduced fusion cross sections for those entrance channels involving projectiles which, on the average, have small binding energies and,

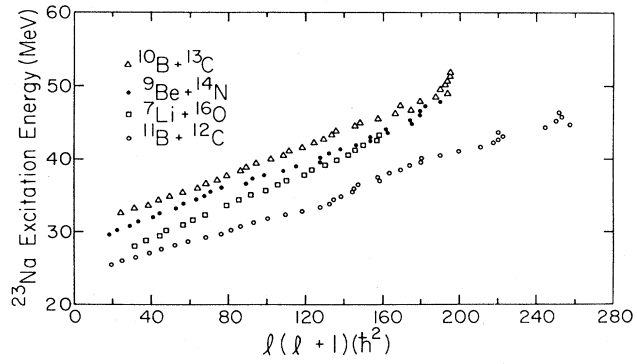

FIG. 12. A comparison of the critical angular momenta for the four entrance channels used to form the ^{23}Na compound nucleus.

TABLE III. Channel spins for entrance channels populating the ^{23}Na compound nucleus.

Channel	Ground state spin ($\hbar$)	Maximum channel spin ($\hbar$)
^{11}B+^{12}C	$\frac{3}{2}^-$,0	$\frac{3}{2}$
^{7}Li+^{16}O	$\frac{3}{2}^-$,0	$\frac{3}{2}$
^{9}Be+^{14}N	$\frac{3}{2}^-$,1^+	$\frac{5}{2}$
^{10}Be+^{13}C	3^+,$\frac{1}{2}^-$	$\frac{7}{2}$

consequently, large breakup strengths. Fusion cross sections have now been measured for a number of different projectiles on ^{12}C and ^{13}C targets (see Table IV and references therein). To compare these systems, we have employed the simplest and most commonly used parametrization of fusion cross sections, the classical equation[21]

$$\sigma_{\rm fus}(E)=\pi R_B^2(1-V_B/E_{\rm c.m.})\,, \tag{4}$$

where R_B and V_B are the barrier radius and potential, respectively. If the total fusion cross section is plotted as a function of $1/E_{\rm c.m.}$, then these two parameters may be extracted from the low-energy data using a simple linear least-squares fitting procedure. It might also be noted that the overall magnitude of the fusion cross section is primarily responsible for determining the value for R_B, while V_B reflects the energy dependence of the cross section.

The entrance channels considered in the present analysis are listed in Table IV. Also presented in this table are the barrier radius and potential parameters for each system. A plot of the barrier radii as a function of target-projectile size, $A_t^{1/3}+A_p^{1/3}$, is presented in Fig. 15. As one might expect, there is a general trend for the barrier radii to increase with increasing size of the target-projectile system. The somewhat unexpected result, however, is that the barrier radii appear to fall along two distinct lines. What is particularly intriguing is that en-

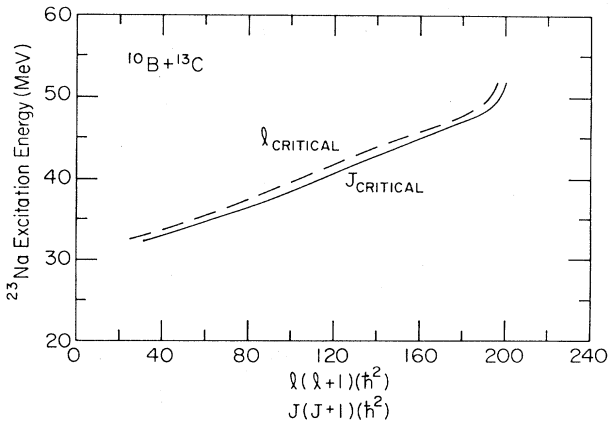

FIG. 13. A comparison of $l_{\rm cr}$ and $J_{\rm cr}$ for the ^{10}B+^{13}C entrance channel.

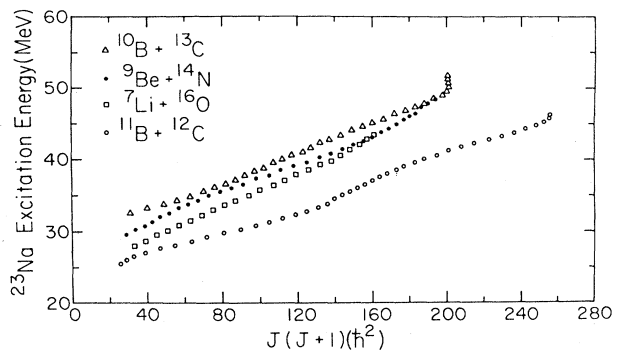

FIG. 14. A comparison of J_{cr} for the four entrance channels used to form the ^{23}Na compound nucleus.

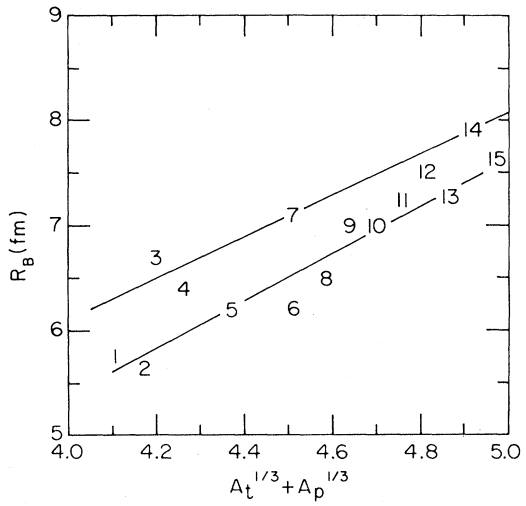

FIG. 15. The barrier radius R_B extracted from fits to the experimental fusion data versus target-projectile size ($A_t^{1/3}+A_p^{1/3}$). The entrance channels used in this figure are listed in Table IV.

trance channels which are very similar, e.g., ^{6}Li+^{12}C and ^{7}Li+^{12}C, ^{6}Li+^{13}C and ^{7}Li+^{13}C, ^{11}B+^{12}C and ^{10}B+^{13}C, and ^{17}O+^{12}C and ^{18}O+^{12}C, have very different barrier radii.

As mentioned previously, the study of the light-particle yields produced by the ^{11}B+^{12}C and ^{10}B+^{13}C reactions suggests a dependence of this yield on the two-particle binding energies of the projectile. Such a process, by competing for total entrance channel flux, would necessarily affect the magnitude of the total fusion cross section. Before attempting to investigate the relationship between projectile binding energy and fusion cross section in this mass region, one must keep in mind that the magnitude of the fusion cross section also depends on the overall size of the target-projectile system (see Fig. 15). To minimize the importance of this effect, only target-projectile systems having similar values of $A_t^{1/3}+A_p^{1/3}$ will be compared, e.g., ^{6}Li+^{13}C and ^{7}Li+^{13}C or ^{14}N+^{12}C and ^{15}N+^{12}C.

TABLE IV. Barrier radii and potentials for various projectiles on ^{12}C and ^{13}C targets.

Label	system	$A_t^{1/3}+A_p^{1/3}$	R_B[a] (fm)	V_B[b] (MeV)	Ref.
1	^{6}Li+^{12}C	4.11	5.7	4.0	13
2	^{6}Li+^{13}C	4.17	5.7	4.2	13
3	^{7}Li+^{12}C	4.20	6.7	4.4	13
4	^{7}Li+^{13}C	4.26	6.4	4.2	13
5	^{9}Be+^{12}C	4.36	6.2	4.0	20
6	^{10}B+^{13}C	4.51	6.2	4.9	11
7	^{11}B+^{12}C	4.51	7.1	5.6	11
8	^{12}C+^{12}C	4.58	6.5	5.8	5
9	^{13}C+^{12}C	4.64	7.0	5.7	5
10	^{14}N+^{12}C	4.70	7.0	6.8	5
11	^{15}N+^{12}C	4.76	7.2	6.3	5
12	^{16}O+^{12}C	4.81	7.5	7.7	5
13	^{17}O+^{12}C	4.86	7.3	7.7	5
14	^{18}O+^{12}C	4.91	7.9	7.7	5
15	^{19}F+^{12}C	4.96	7.6	8.0	5

[a]Uncertainties in R_B are approximately 0.3 fm.
[b]Uncertainties in V_B are approximately 0.5 MeV.

The two-particle binding energies of the projectiles involved in the present study are listed in Table V. Inspection of the lithium binding energies reveals that, on the average, the ^{6}Li nucleus is more weakly bound than the ^{7}Li nucleus and should, therefore, be more likely to dissociate into two fragments before fusion can occur. Consistent with this interpretation is the fact that the fusion cross sections for reactions induced by ^{6}Li projectiles are smaller than those induced by ^{7}Li (as evidenced by smaller values of R_B for ^{6}Li projectiles in Fig. 15). In the case of the boron nuclei, ^{10}B is more weakly bound than ^{11}B and should, therefore, more readily dissociate into light fragments. In agreement with this conclusion are the results of an experiment which measured the light-particle yield for the ^{11}B+^{12}C and ^{10}B+^{13}C entrance channels at 54 MeV (integrated light particle cross sections of 193 and 290 mb were attributed to projectile breakup for the ^{11}B+^{12}C and ^{10}B+^{13}C systems, respectively).[12] In addition, the entrance channel which involves the ^{10}B projectile has the smaller fusion cross section [at 54 MeV, the ^{10}B+^{13}C fusion cross section was 890 mb, while the ^{11}B+^{12}C was 1064 mb (Refs. 10 and 11)]. For the reactions involving either carbon or nitrogen projectiles, the case is not clear. Inspection of the carbon binding energies reveals that both have relatively weakly bound configurations which may account for the reduced fusion cross sections observed for both projectiles. The fusion cross sections for the systems involving both ^{14}N and ^{15}N projectiles are also found to be small (both have barrier radii falling on the lower line). Again, neither system appears to be favored in terms of the projectile binding energy and one might expect, therefore, to find similar fusion cross sections. Finally, inspection of the oxygen induced reactions reveals that the ^{17}O projectile produces fusion cross sections which are reduced relative to those of both ^{16}O and ^{18}O. In Table V one finds that ^{17}O is more weakly bound than either ^{16}O or ^{18}O. The above systematics suggest that the fusion cross sections and the associated bar-

TABLE V. Projectile binding energies. The light member of each breakup pair is listed at the top of each column.

Projectile	n	p	d	t	^{3}He	α
^{6}Li	5.7	4.6	1.5	15.8		
^{7}Li	7.3	10.0	9.6	2.5	25.9	
^{10}B	8.4	6.6	6.0	18.7	17.8	4.5
^{11}B	11.5	11.2	15.8	11.2	27.2	8.7
^{12}C	18.7	16.0	25.2	27.4	26.3	7.4
^{13}C	4.9	17.5	18.7	23.9	24.4	10.6
^{14}N	10.6	7.6	10.3	22.7	20.7	11.6
^{15}N	10.8	10.2	16.2	14.8	28.2	11.0
^{16}O	15.7	12.1	20.7	25.0	22.8	7.2
^{17}O	4.1	13.8	14.0	18.6	18.8	6.4
^{18}O	8.0	15.9	19.6	15.8	25.6	6.2

rier radii parameters simply reflect the degree to which a projectile will dissociate before fusion can occur.

IV. CONCLUSIONS

The fusion cross sections for four entrance channels leading to the ^{23}Na compound nucleus have been studied. From the total fusion cross sections for these systems, the energy dependence of the critical angular momentum for each entrance channel has been deduced. A plot of these critical angular momenta versus ^{23}Na excitation energy reveals that a property of the compound nucleus, like the yrast or statistical yrast line, cannot be responsible for the fusion cross section limitations. A previous study of the light particles produced in the ^{11}B+^{12}C and ^{10}B+^{13}C reactions, along with a systematic study of fusion cross sections in this mass and energy region, suggests that the fusion cross section limitation is at least partly due to a competing reaction mechanism, projectile breakup.

*Present address: Physics Department, Michigan State University, East Lansing, MI 48824.

[1]R. Bass, Phys. Rev. Lett. **39**, 265 (1977).
[2]D. Horn and A. J. Ferguson, Phys. Rev. Lett. **41**, 1529 (1978).
[3]H. J. Krappe and J. R. Nix, in *Proceedings of the Third International Atomic Energy Symposium on the Physics and Chemistry of Fission, Rochester, 1973* (IAEA, Vienna, 1974), p. 159.
[4]S. M. Lee, T. Matsuse, and A. Arima, Phys. Rev. Lett. **45**, 165 (1980).
[5]D. G. Kovar, D. F. Geesaman, T. H. Braid, Y. Eisen, W. Henning, T. R. Ophel, M. Paul, K. E. Rehm, S. J. Sanders, P. Sperr, J. P. Schiffer, S. L. Tabor, S. Vigdor, and B. Zeidman, Phys. Rev. C **20**, 1305 (1979), and references therein.
[6]J. Gomez del Campo, R. A. Dayras, J. A. Biggerstaff, D. Shapira, A. H. Snell, P. H. Stelson, and R. G. Stokstad, Phys. Rev. Lett. **43**, 26 (1979).
[7]J. P. Wieleczko, S. Harar, M. Conjeaud, and F. Saint-Laurent, Phys. Lett. **93B**, 35 (1980).
[8]F. Saint-Laurent, M. Conjeaud, and S. Harar, Nucl. Phys. **A327**, 517 (1979).
[9]L. C. Dennis and S. T. Thornton, Phys. Rev. C **22**, 340 (1980).
[10]J. F. Mateja, A. D. Frawley, L. C. Dennis, K. Abdo, and K. W. Kemper, Phys. Rev. Lett. **47**, 311 (1981).
[11]J. F. Mateja, A. D. Frawley, L. C. Dennis, K. Abdo, and K. W. Kemper, Phys. Rev. C **25**, 2963 (1982).
[12]J. F. Mateja, J. Garman, and A. D. Frawley, Phys. Rev. C **28**, 1579 (1983).
[13]L. C. Dennis, K. Abdo, A. D. Frawley, and K. W. Kemper, Phys. Rev. C **26**, 981 (1982).
[14]A. C. Xenoulis, A. E. Aravantinos, C. J. Lister, J. W. Olness, and R. L. Kozub, Phys. Lett. **106B**, 461 (1981).
[15]J. E. Poling, E. Norbeck, and R. R. Carlson, Phys. Rev. C **13**, 648 (1976).
[16]J. A. Kuehner and E. Almquist, Phys. Rev. **134**, B1229 (1964).
[17]J. S. Eck, J. R. Leih, T. R. Ophel, and P. D. Clark, Phys. Rev. C **21**, 2352 (1980).
[18]M. E. Ortiz, J. Gomez del Campo, Y. D. Chan, D. E. Gregorio, J. L. C. Ford, Jr., D. Shapira, R. G. Stokstad, J. P. F. Sellschop, R. L. Parks, and D. Weiser, Phys. Rev. C **25**, 1436 (1982).
[19]P. A. De Young, J. J. Kolata, L. J. Satkowiak, and M. A. Xapsos, Phys. Rev. C **26**, 1482 (1982).
[20]L. C. Dennis (private communication).
[21]H. H. Gutbrod, M. Blann, and W. G. Winn, Nucl. Phys. **A213**, 267 (1973).